APPLICATION OF FRACTIONAL ALGORITHMS IN THE CONTROL OF A TWIN ROTOR MULTIPLE INPUT-MULTIPLE OUTPUT SYSTEM

J. Coelho[1], R. Matos Neto[1], C. Lebres[1], Victor Santos[1], N. M. Fonseca Ferreira[1]
E. J. Solteiro Pires[2], J. A. Tenreiro Machado[3]
[1]Polytechnic Institute of Coimbra, Institute of Engineering of Coimbra,
Dept. of Electrical Engineering, Quinta da Nora, Apartado 10057
3031-601 Coimbra Codex, Portugal,
[2]University of Trás-os Montes e Alto-Douro, Dept. of Engineering Quinta de Prados,
Apartado 202, 5000 Vila Real, Portugal
[3]Polytechnic Institute of Porto, Institute of Engineering of Porto,
Rua Dr Ant. Bernardino de Almeida, 4200–072 Porto, Portugal,
[1]e-mail: {clebres, vsantos, nunomig}@isec.pt, [2]email: epires@utad.pt, [3]e-mail: jtm@isep.ipp.pt

ABSTRACT
This paper presents the modelling and control of a laboratory helicopter twin rotor *MIMO* system using the *MatLab* package. Firstly, we provide an overview of the system model, secondly, we compare the behaviour of fractional and integer order controllers used a *PSO* algorithm for the controller optimization in order to obtain the minimum error. Finally, we analyse the system performance and the results obtained with the real helicopter show that fractional algorithms are smoother than conventional *PID*. Both controllers reveal good output responses but the *PID* needs more energy to perform the same task.

KEY WORDS
Helicopter, Mathematical Model, Position Control, Fractional Control, Particle Swarm Optimization.

1. Introduction

This paper presents several control techniques for a laboratory helicopter model. We adopt the Twin Rotor Mimo System (Feedback – TRMS) [1] and we compare the results of integer and fractional order control algorithms. We consider the dynamics of the helicopter system with two degrees of freedom (*dof*) [2, 3] and present several real-time experiments of the closed loop system.
Figure 1 shows a laboratory model of the Twin Rotor in two different views. The beam is joined to its base through an articulation and has two propellers driven by DC motors. This articulated joint allows the beam to rotate so that its ends move on spherical surfaces. A counter-weight fixed to the beam determines a stable equilibrium position.
The rotors are positioned perpendicularly to each other, so that the movements in the vertical and horizontal planes are affected by the thrust of one propeller.

Figure 1 - Two views of the twin rotor MIMO system.

The control signals consist in the input voltages of the DC motors. The measured signals are the two position angles that determine the position of the beam in the space, and the angular velocities of the rotors. The positions are measured using incremental encoders, and the angular velocities are reconstructed by a simple differentiation with a second-order filtering of the measured angles.
The paper is organized as follow. Section two gives an overview of the system model. Section three discusses the conventional integer and the fractional order algorithms. Sections four and five present the particle swarm optimization and the controller's parameters optimization, respectively. Section six analyses the simulations results. Finally, section seven outlines the main conclusions.

2. Mathematical Model

The helicopter has two *dof*, namely, the rotation of the helicopter body with respect to the horizontal axis and the rotation around the vertical axis. Each axis has one potentiometer for measuring the correspondent angle. The helicopter can move in the range $-170^{\circ} < \alpha_h < 170^{\circ}$, and $-60^{\circ} < \alpha_v < 60^{\circ}$, around the horizontal and vertical axis, respectively. The inputs of the model are the motor voltages U_h and U_v affecting the main and tail rotors. The output command must match the capabilities of the hardware board that is capable to outputing a [0, 5] Volt signal. This signal is shifted in the amplifier to create ±2.5 Volt capability required to command the drive motor in

both directions. When no control signals are applied, the helicopter will tend to position at $\alpha_h = -60^o$.

Table 1 – List of symbols

Variable	Description	Units [SI]
α_h	Horizontal position (azimuth position) of the model beam	[rad]
Ω_h	Angular velocity (azimuth velocity) of the model beam	[rad/s]
U_h	Horizontal DC-motor voltage control input	[V]
G_h	Linear transfer function of tail rotor DC-motor	
H	Non-linear part of DC- motor with tail rotor	[rad/s]
ω_h	Rotational speed of tail rotor	[rad/s]
F_h	Non-linear function (quadratic) of aerodynamic force from tail rotor	[N]
l_h	Effective arm of aerodynamic force from tail rotor	[m]
J_h	Non-linear function of moment of inertia with respect to vertical axis	[Kg.m^2]
M_h	Horizontal turning torque	[Nm]
K_h	Horizontal angular momentum	[Nm.s]
f_h	Moment of friction force in vertical axis	[Nm]
α_v	Vertical position (Pitch position) of the model beam	[rad]
Ω_v	Angular velocity (Pitch velocity) of the model beam.	[rad/s]
U_v	Vertical DC-motor voltage control input	[V]
G_v	Linear transfer function of main rotor DC-motor	
v	Non-linear part of DC-motor with main rotor	[rad/s]
ω_v	Rotational speed of main rotor	[rad/s]
F_v	Non-linear function (quadratic) of aerodynamic force from main rotor	[N]
l_v	Arm of aerodynamic force from main rotor	[m]
J_v	Moment of inertia with respect to horizontal axis	[Kg.m^2]
M_v	Vertical turning moment	[Nm]
K_v	Vertical angular momentum	[Nm.s]
f_v	Moment of friction force in horizontal axis	[Nm]
f	Vertical turning moment from counterbalance	[Nm]
J_{hv}	Vertical angular momentum from tail rotor	[Nm.s]
J_{vh}	Horizontal angular momentum from tail rotor	[Nm.s]
g_{vh}	Non-linear function (quadratic) of reaction turning	[Nm]
g_{hv}	Non-linear function (quadratic) of reaction turning	[Nm]
t	Time	[s]
L	Laplace Operator	
s	Laplace variable	
z	Z Transform variable	

The physical model is developed under some simplifying assumptions [4]. It is assumed that friction is of viscous type and that the propeller air subsystem can be described in accordance with the postulates of flow theory.
First, we consider the rotation of the beam in the vertical plane, around the horizontal axis. Having in mind that driving torques are produced by the propellers, the rotation can be described by the pendulum motion principle. From the Newton second law of motion we obtain:

$$M_v = J_v \frac{d^2\alpha_v}{dt^2} \tag{1}$$

$$M_v = \sum_{i=1}^{4} M_{vi} \tag{2}$$

$$J_v = \sum_{i=1}^{8} J_{vi} \tag{3}$$

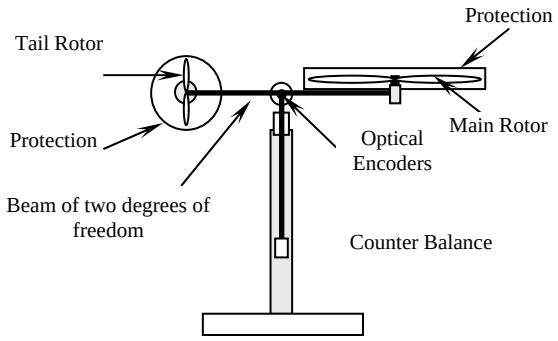

Figure 2 – The twin rotor mimo system.

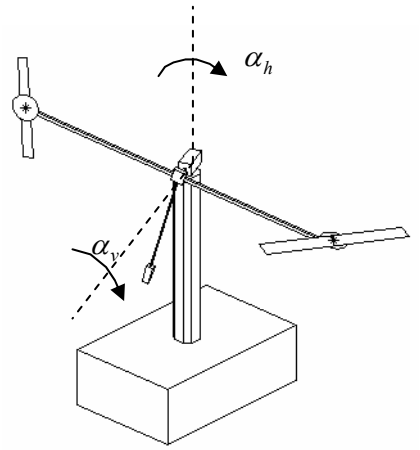

Figure 3 – The rotation of the helicopter system.

Tables 1 and 2 depict the list of symbols and the helicopter parameters, respectively. To determine the moments of gravity applied to the beam, making it to rotate around the horizontal axis, we consider the situation of in figure 4, and:

$$M_{v1} = g[A - B]\cos\alpha_v - C\sin\alpha_v \tag{4a}$$

$$A = \left(\frac{m_t}{2} + m_{tr} + m_{ts}\right) l_t \tag{4b}$$

$$B = \left(\frac{m_m}{2} + m_{mr} + m_{ms}\right) l_m \tag{4c}$$

$$C = \frac{m_b}{2} l_b + m_{cb} l_{cb} \tag{4d}$$

Table 2 – The parameters of the Helicopter

Variable	Value	Units[SI]
m_{mr}	0.228	[kg]
m_{m}	0.0145	[kg]
m_{tr}	0.206	[kg]
m_t	0.10166	[kg]
m_{cb}	0.068	[kg]
m_b	0.022	[kg]
m_{ms}	0.225	[kg]
m_{ts}	0165	[kg]
l_m	0.24	[m]
l_t	0.25	[m]
l_b	0.26	[m]
l_{cb}	0.13	[m]
r_{ms}	0.155	[m]
r_{ts}	0.10	[m]

where r_{ms} is the radius of the main shield and r_{ts} is the radius of the tail shield.

Also:

$$M_{v2} = l_m F_v(\omega_m) \tag{5}$$

where $F_v(\omega_m)$ denotes the dependence of the propulsive force on the angular velocity of the rotor.

$$M_{v3} = -\Omega_h^2 (A + B + C) \sin\alpha_v \cos\alpha_v \tag{6}$$

$$\Omega_h = \frac{d\alpha_h}{dt} \tag{7}$$

To determine the moments of propulsive forces applied to the beam consider the situation given in figure 4.
Finaly:

$$M_{v4} = -\Omega_v K_v \tag{8}$$

$$\Omega_v = \frac{d\alpha_{vh}}{dt} \tag{9}$$

where Ω_v is the angular velocity around the horizontal axis and K_{v} is a constant.

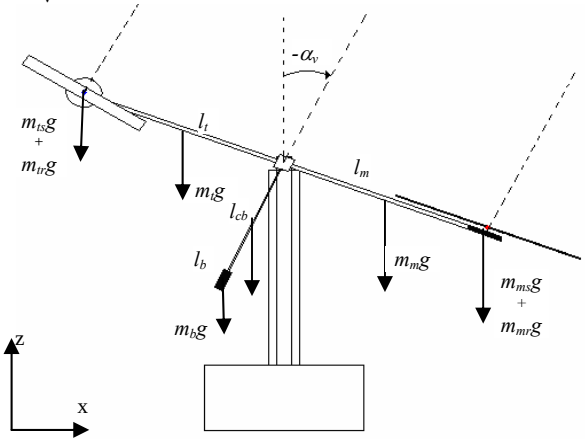

Figure 4 – Gravity forces in the TRMS, corresponding to the return torque, which determine the equilibrium position of the system.

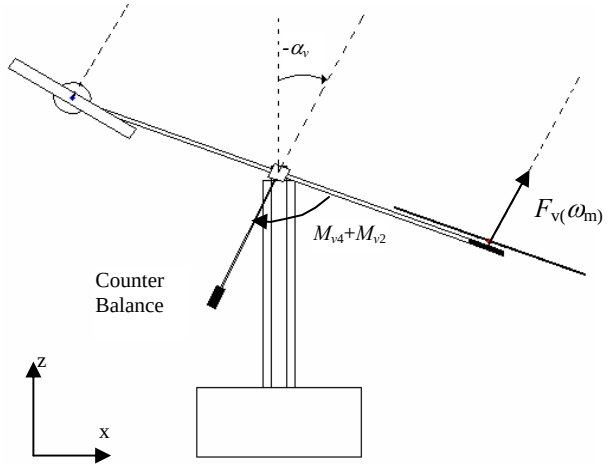

Figure 5 – Propulsive force moment and friction moment in the TRMS.

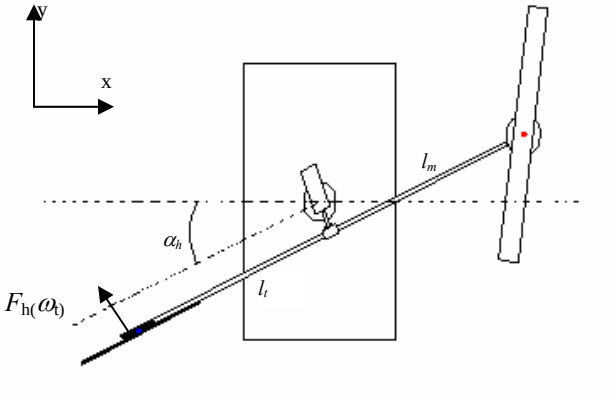

Figure 6 – Moments of forces in horizontal plane.

According to figure 6 we can determine components of the moment of inertia relative to the horizontal axis yielding:

$$J_{v1} = m_{mr} l_m^2 \tag{10a}$$

$$J_{v2} = m_m \frac{l_m^2}{3} \tag{10b}$$

$$J_{v3} = m_{cb} l_{cb}^2 \tag{10c}$$

$$J_{v4} = m_b \frac{l_b^2}{3} \tag{10d}$$

$$J_{v5} = m_{tr} l_t^2 \tag{10e}$$

$$J_{v6} = m_t \frac{l_t^2}{3} \tag{10f}$$

$$J_{v7} = \frac{m_{ms}}{2} r_{ms}^2 + m_{ms} l_m^2 \tag{10g}$$

$$J_{v8} = m_{ts} r_{ts}^2 + m_{ts} l_t^2 \tag{10h}$$

Notice, that this moment is independent of the position of the beam.

Similarly, we can describe the motion of the beam around the vertical axis, having in mind that the driving torques are produced by the rotors and that the moment of inertia depends on the pitch angle of the beam. The horizontal motion of the beam (around the vertical axis) can be described as a rotational motion of a solid mass:

$$M_h = J_h \frac{d^2\alpha_h}{dt^2} \tag{11a}$$

$$M_h = \sum_{i=1}^{2} M_{hi} \tag{11b}$$

$$J_h = \sum_{i=1}^{8} J_{hi} \tag{11c}$$

To determine the moments of forces applied to the beam, making it to rotate around the vertical axis, we consider the situation shown in Figure 6, yielding:

$$M_{h1} = l_t . F_h(w_t) \cos\alpha_v \tag{12}$$

where $F_h(\omega_t)$ denotes the dependence of propulsive force on the angular velocity of the tail rotor, and:

$$M_{h2} = -\Omega_h K_h \tag{13}$$

$$J_h = D\cos^2\alpha_v + E\sin^2\alpha_v + F \tag{14}$$

$$D = \frac{m_b}{3} l_b^2 + m_{cb} l_{cb}^2 \tag{15}$$

$$E = \left(\frac{m_m}{3} + m_{mr} + m_{ms}\right) l_m^2 + \left(\frac{m_t}{3} + m_{tr} + m_{ts}\right) l_t^2 \tag{16}$$

$$F = m_{ms} r_{ms}^2 + \frac{m_{ts}}{2} r_{ts}^2 \tag{17}$$

The helicopter motion can be describe by the equations:

$$\frac{dS_v}{dt} = \frac{l_m F_v(\omega_m) - \Omega_v K_v + G - H}{J_v} \tag{18a}$$

$$G = g\left[(A-B)\cos\alpha - C\sin\alpha_v\right] \tag{18b}$$

$$H = \frac{1}{2}\Omega_h^2 (A+B+C)\sin 2\alpha_v \tag{18c}$$

$$\frac{d\alpha_v}{dt} = \Omega_v \tag{18d}$$

$$\Omega_v = \frac{S_v + J_{tr}\omega_t}{J_v} \tag{18e}$$

$$\frac{dS_h}{dt} = \frac{l_t F_h(\omega_t)\cos\alpha_v - \Omega_h K_h}{J_h} \tag{18f}$$

$$\Omega_h = \frac{d\alpha_h}{dt} \tag{18g}$$

$$\Omega_h = S_h + \frac{J_{tmr}\omega_m \cos\alpha_v}{J_h} \tag{18h}$$

The angular velocities depend on the DC motors:

$$\frac{du_{vv}}{dt} = \frac{1}{T_{mr}}\left(-u_{vv} + u_v\right) \tag{19a}$$

$$\omega_m = P_v(u_{vv}) \tag{19b}$$

$$\frac{du_{hh}}{dt} = \frac{1}{T_{tr}}\left(-u_{hh} + u_h\right) \tag{19c}$$

$$\omega_t = P_h(u_{hh}) \tag{19d}$$

Finally, the mathematical model becomes a set of six non-linear equations, namely:

$$\mathbf{U} = \left[U_h \; U_v\right]^T \tag{20}$$

$$\mathbf{X} = \left[S_h \; \alpha_h \; u_{hh} \; S_v \; \alpha_v \; u_{vv}\right]^T \tag{21}$$

$$\mathbf{Y} = \left[\Omega_h \; \alpha_h \; \omega_t \; \Omega_v \; \alpha_v \; \omega_m\right]^T \tag{22}$$

where **U** is the input, **X** is the state and **Y** is the output vector and can see in Figure 7.

3. Twin Rotor Mimo Controllers

3.1. Integer Order Algorithms

The *PID* controllers are the most commonly used control algorithms in industry. Among the various existent schemes for tuning *PID* controllers, the Ziegler-Nichols (*Z-N*) method is the most popular and is still extensively used for the determination of the *PID* parameters. It is well known that the compensated systems, with controllers tuned through this method, have generally a step response with a high percent overshoot. Moreover, the *Z-N* heuristics are only suitable for plants with monotonic step response [5-7].

The transfer function of the *PID* controller is:

$$G_c(s) = \frac{U(s)}{E(s)} = K\left(1 + \frac{1}{T_i s} + T_d s\right) \tag{23}$$

where $E(s)$ is the error signal and $U(s)$ is the controller's output. The parameters K, T_i, and T_d are the proportional gain, the integral time constant and the derivative time constant of the controller, respectively.
The design of the *PID* controller consist on the determination of the optimum *PID* parameters (K, T_i, T_d) that minimize J, the integral of the square error (*ISE*), defined as:

$$J = \int_0^\infty \left\{\left[\alpha_h(t) - \alpha_{hr}(t)\right]^2 + \left[\alpha_v(t) - \alpha_{vr}(t)\right]^2\right\} dt \tag{24}$$

where $\alpha_i(t)$ is the step response of the closed-loop system with the *PID* controller and $\alpha_{ir}(t)$ is the desired step response. The control architecture can be resumed in the block diagram of Figure 8, with the two independent controllers

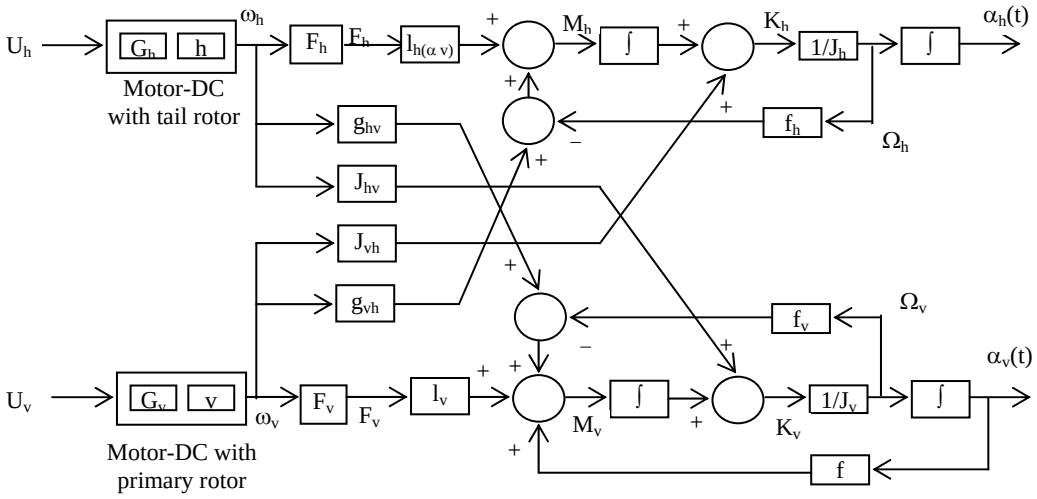

Figure 7 – The MIMO block diagram of the twin rotor

3.2. Fractional Order Algorithms

In this section we present the Fractional Order (*FO*) algorithms adopted in the two control loops.
The mathematical definition of a derivative of fractional order α has been the subject of several different approaches. For example, we can mention the Laplace and the Grünwald-Letnikov definitions:

$$D^{\alpha}[x(t)] = L^{-1}\{s^{\alpha} X(s)\} \tag{25a}$$

$$D^{\alpha}[x(t)] = \lim_{h\to 0}\left[\frac{1}{h^{\alpha}}\sum_{k=1}^{\infty}\frac{(-1)^k\Gamma(\alpha+1)}{\Gamma(k+1)\Gamma(\alpha-k+1)}x(t-kh)\right] \tag{25b}$$

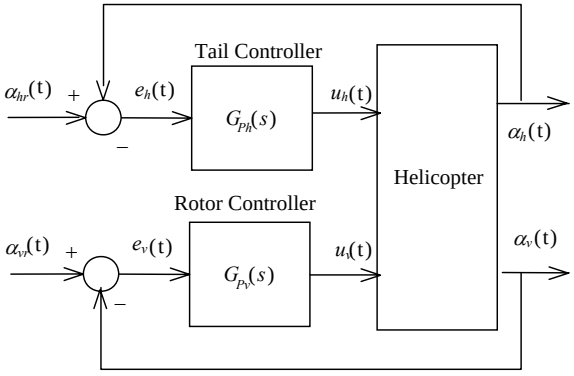

Figure 8 –Twin Rotor Mimo block *PID* control diagram

where Γ is the gamma function and *h* is the time increment.
In our case, for implementing *FO* algorithms of the type PID^{α}, $C(s) = K_P + \frac{K_i}{T_i s} + K_D s^{\alpha}$, $0 \le \alpha_i \le 1$, we adopt a 4th-order discrete-time Pade approximation ($a_i, b_i, c_i, d_i \in \Re$, $k = 4$):

$$C_{Ph}(z) \approx K_{Ph}\frac{a_0 z^k + a_1 z^{k-1} + .. + a_k}{b_0 z^k + b_1 z^{k-1} + ... + b_k} \tag{26a}$$

$$C_{Pv}(z) \approx K_{Pv}\frac{c_0 z^k + c_1 z^{k-1} + .. + c_k}{d_0 z^k + d_1 z^{k-1} + ... + d_k} \tag{26b}$$

where K_{Ph} and K_{Pv} are the tail and rotor controller gains, respectively.

4. Particle Swarm Optimization

Particle swarm optimization (PSO) algorithm was developed by Kennedy and Eberhart in 1995 [11]. This optimization technique, based on a population search, is inspired by social behavior of bird flocking fish schooling. An analogy is established between a particle and an element of swarm. These particles fly trough the search space following current optimum particles. In each algorithm iteration, a particle movement is characterized by two vectors representing its current position *x* and velocity *v*.

The velocity, of a particle, is changed according the cognitive knowledge *b* (the best solution found so far by the particle) and the social knowledge *g* (the best solution found by the swarm). The weight of each knowledge, in the velocity update, is different according with the random values ϕ_i, $i = \{1, 2\}$. Theses values are random factor follow a probabilistic uniform low $\phi_i \sim U[0, \phi_{i\,max}]$

Initialize Swarm
repeat
  forall particles *do*
    Calculate fitness *f*
  end
  forall particles *do*
    $v_{t+1} = I\, v_t + \phi_1(b\text{-}x) + \phi_2(g\text{-}x)$
    $x_{t+1} = x_t + v_{t+1}$
  end
until stopping criteria

Figure 9 – Particle Swarm Optimization

where I and t are the inertia and the iteration time respectively.

PSO is a very attractive technique among many other population based algorithms, because it has only a few parameters to adjust. PSO have been used with success in a vast number of applications, such as robotics [12, 13] and electrical systems [14]. In this paper the PSO will be adopted in the controller tunning.

5. Parameters Optimization

In this section is used a *PSO* algorithm for the controller optimization. The *PSO* determines the optimal parameters, K_p, K_d and K_i, of the control system, in order to obtain the minimum error when the helicopter moves between two workspace points. Since the parameters of the model are unknown, the *PSO* will evaluate the fitness particles of the real system. Therefore, to evaluate each particle, the *PSO* sends the command with the particle parameters to the helicopter in order to move it and the position error is measured.

In the experiments it is adopted $\phi_{i\ max} = 1.6$ and 10 particle population during 100 iterations. The parameter space is shown in Table 3. The helicopter moves between the point $A \equiv \{0^o, 0^o\}$ degrees up to the point $B \equiv \{12^o, 0^o\}$ for main rotor perturbation and moves between the point $A \equiv \{0^o, 0^o\}$ degrees up to the point $B \equiv \{0^o, 12^o\}$ for tails perturbation. Table 4 depicts the final values obtained for each gain.

6. Controller Performances

This section analyzes the system response under the control action of the classical *PID* and PID^{α} algorithms.

In order to study the system dynamics we apply, separately, rectangular pulses, at the tail and main rotor references, that is, we perturb the reference with $\{\delta\alpha_h, \delta\alpha_v\} = \{12^o, 0^o\}$ and $\{\delta\alpha_h, \delta\alpha_v\} = \{0^o, 12^o\}$. These perturbations have an duration of 15 seconds. The experimental results are presented here to compare the closed loop performance of the Integer Order (*IO*) and Fractional Order (*FO*) control algorithms.

The *PSO* determines the optimal parameters of the controller and replace them in the helicopter.

Figure 10 and Table 5 analyze of the time response characteristics, for the tail and the rotor perturbations and depict the statistics, of the voltage amplitudes for the perturbation $\delta\alpha_v$ and $\delta\alpha_h$.

Figures 11 and 12 show the required voltages U_v and U_h to execute the task.

The PID^{α} controller reveals better performance, namely is faster and produces smaller errors than the *PID*. The time response of the PID^{α} controller presents a softer response a smaller overshoot and reduces the strong effect of the input and output cross coupling.

In figure 11 it is shown the effect of the motor saturation in the amplifier, in the ±2.5 Volt ranges required to command the drive motor in both directions. For a pulse perturbation at the $\alpha_{hr} = 12^o$ the *PID* requires larger U_v voltages than the PID^{α}. For a pulse perturbation $\alpha_{vr} = 12^o$ the required U_v voltages for one *PID* and PID^{α} are almost identical, but for the horizontal axis the PID^{α} need more U_h voltage than the *PID*.

7. Conclusions

In this paper a two rotor MIMO helicopter system is studied and several experiments are developed. The mathematical model of TRMS is derived, and its dynamical characteristics, such as equilibrium position, propeller thrust and gravity compensation are analyzed. For this system are compared integer and fractional algorithms. The results of the PID^{α} controller reveal better performances than the classical integer order controller.

References

[1] Feedback Instruments *Ltd Manual: 33-007-1C* Ed04. 2002.

[2] J. Gordon Leishman. *Principles of Helicopter Aerodynamics*. Second Edition, Cambridge University Press.

[3] Martin D. Maisel. Demo J. Giulianetti and Daniel C. Dugan, *The History of the XV-15 Tilt Rotor Research Aircraft From Concept to Flight*. National Aeronautics and Space Administration Office of Policy and Plans NASA History Division Washington. D.C.2000.

[4] M. López Martínez. F.R. Rubio. *Approximate Feedback Linearization of a Laboratory Helicopter*, Sixth Portuguese Conference on Automatic Control. pp.43-45, Faro, Portugal, 2004.

[5] Åström. K.. Hang. C.. Persson. P. and Ho.W., *Towards intelligent PID control*. Automática 28(1), pp. 1–9, 1992.

[6] Åström. K. J. and Wittenmark. B. (1984). *Computer Controlled Systems. theory and Design*. Prentice-Hall. Englewood Cliffs.

[7] Podlubny. *Fractional Differential Equations.* Academic Press. San Diego. 1999.

[8] K. S. Miller and B. Ross. *An Introduction to the Fractional Calculus and Fractional Differential Equations.* Wiley & Sons. New York. 1993.

[9] A. Oustaloup. *La Commande CRONE: Commande Robuste d'Ordre Non Entier.* Editions Hermès. Paris. 1991.

[10] Machado. J. A. T.. *Discrete-Time Fractional-Order Controllers.* FCAA J. of Fractional Calculus & Applied Analysis Vol. 4; pp. 47–66. 2001.

[11] J. Kennedy and R. C. Eberhart. Particle swarm optimization. In Proceedings of the 1995 IEEE International Conference on Neural Networks. volume 4. pp. 1942–1948. Perth. Australia. IEEE Service Center. Piscataway. NJ. 1995.

[12] J. Tang. J. Zhu. and Z. Sun. "A novel path panning approach based on appart and particle swarm optimization. In LNCS. editor. Proceedings of the 2nd International Symposium on Neural Networks. volume 3498. 2005.

[13] E. J. Solteiro Pires. P. B. de Moura Oliveira. J. A. Tenreiro Machado. J. Boaventura Cunha. "Particle Swarm Optimization versus Genetic Algorithm in Manipulator Trajectory Planning". The 7th Portuguese Conference on Automatic Control, pp.230. 11-13 September, Lisbon, Portugal, 2006.

[14] M. R. Alrashidi. M. E. El-Hawary. "A Survey of Particle Swarm Optimization Applications in Power System Operations". Electric Power Components and Systems. 34:12. 1349 - 1357 Taylor & Francis.

Table 3. Initial limits for each gain.

		k_p	k_i	k_d	α_r	α_t
PID	Main rotor	[20-10]	[15-5]	[10-5]		
	Tail rotor	[15-5]	[5-1]	[10-5]		
PID^{α}	Main rotor	[0.1-10]	[0.1-10]	[0.1-20]	[0.7-0.9]	[0.7-0.9]
	Tail rotor	[0.01-10]	[0.1-10]	[90-110]	[0.7-0.9]	[0.7-0.9]

Table 4. The final values for each gain.

	Pulse perturbation		K_p	K_i	K_d	α_r	α_t
PID	Main rotor	Main rotor	14.939	5.1871	6.1128		
		Tail rotor	9.5506	2.2457	9.4216		
	Tail	Main rotor	13.802	11.309	6.7889		
		Tail rotor	10.806	1.2375	7.8844		
PID^{α}	Main rotor	Main rotor	1.2041	2.4074	4.0891	0.8777	0.8772
		Tail rotor	0.7691	6.9722	98.272		
	Tail	Main rotor	3.7969	3.9100	3.9135	0.8716	0.8893
		Tail rotor	0.5593	3.6052	99.507		

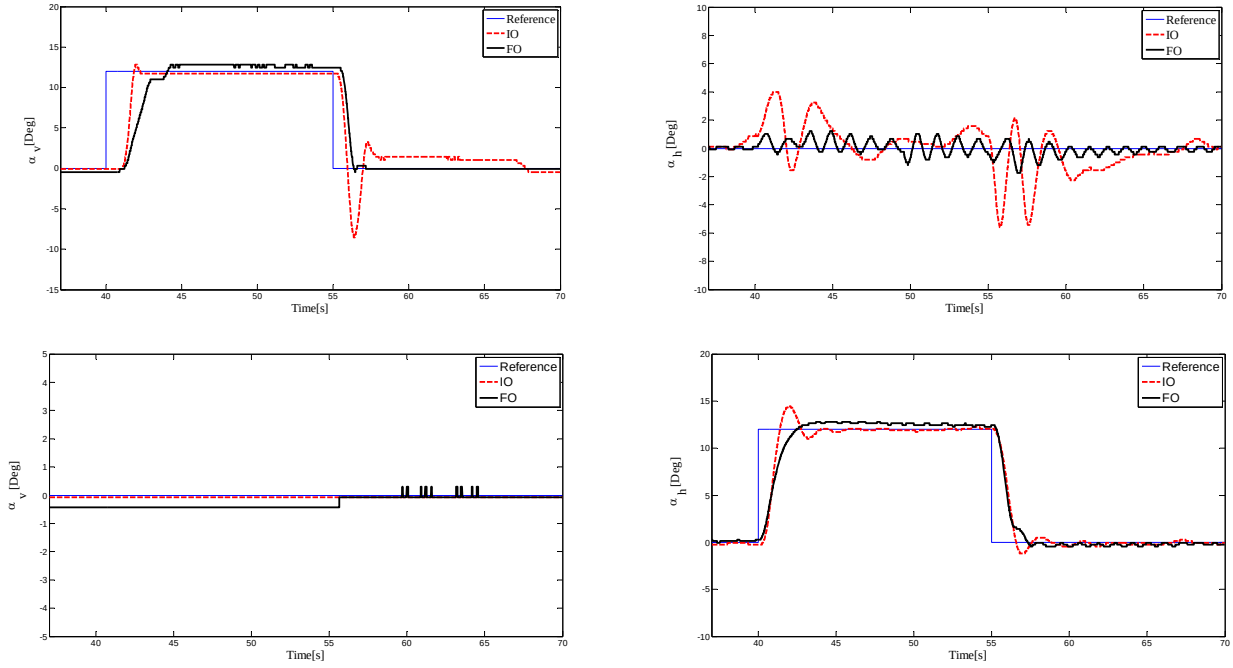

Figure 9 – Time responses of the experimental 2–dof helicopter for α_v and α_h using the *PID* and PID^{α} controllers, for a pulse perturbation at the α_{hr} = 12º and α_{vr} = 12º position reference for sampling time h = 0.01 s.

Table 5. Time response and statistical analysis characteristics for $\delta\alpha_v$ and $\delta\alpha_h$ at the reference.

	PO%	*ess* [deg]	*Tp* [s]	*Ts* [s]	$U_v(Mean)$	$U_h(Mean)$	σ_v	σ_h	$\delta\alpha_v$	$\delta\alpha_h$
PID	2.265	0.29	1.79	2.28	1.3404	0.1330	0.9374	0.9275	1	0
	20.58	0.079	1.89	2.02	1.3626	0.4274	0.5525	0.7728	0	1
PID^{α}	2.265	0.82	4.05	4.26	1.3545	0.2274	0.4972	1.3922	1	0
	6.83	0.820	3.76	4.31	1.2619	0.4488	0.3881	1.0396	0	1

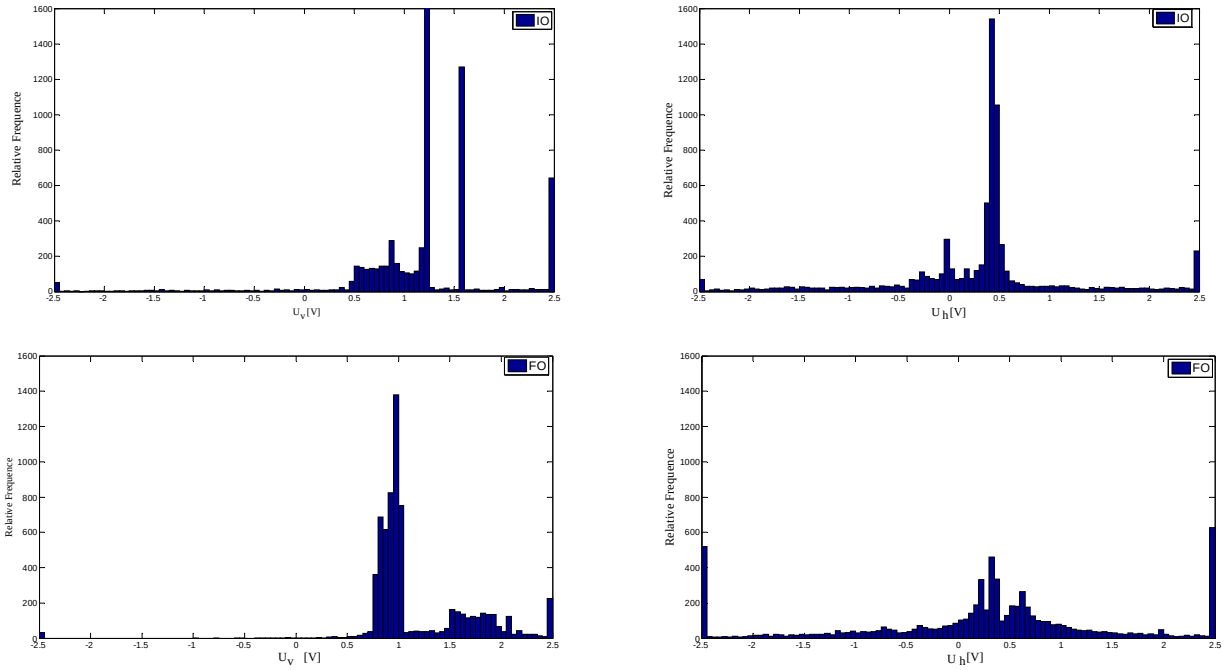

Figure 10 – The experimental 2–*dof* helicopter rotor and tail voltage statistical distribution using the *PID vs PID*$^{\alpha}$ controllers, for a pulse perturbation $\delta\alpha_v = 12^o$ at the α_{vr} position reference for sampling time $h = 0.01$ s.

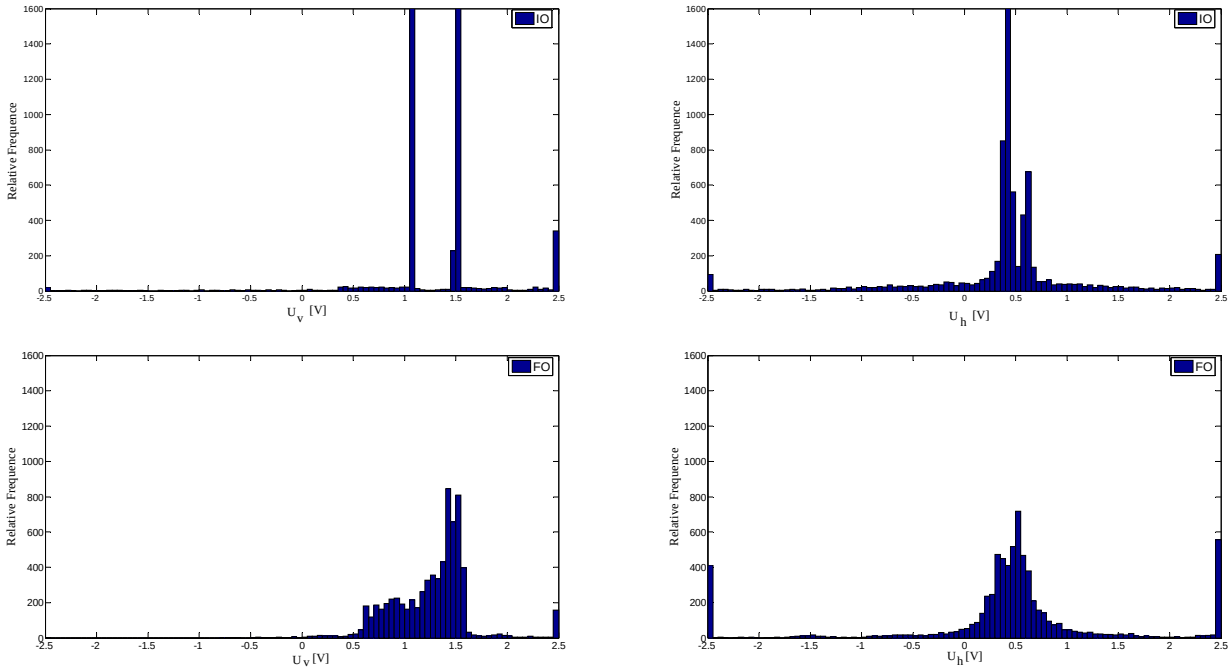

Figure 11 – The experimental 2–*dof* helicopter rotor and tail voltage statistical distribution using the *PID vs PID*$^{\alpha}$ controllers, for a pulse perturbation $\delta\alpha_h = 12^o$ at the α_{hr} position reference for sampling time $h = 0.01$ s.